Chapter- 4

Provenance of Mid-Holocene Sediments in the Great Rann of Kachchh

4.1 Introduction

At the western margin of the Indian subcontinent lies a unique Quaternary terrain known as the Great Rann of Kachchh (GRK). The GRK can be described as a vast expanse of monotonously flat, salt encrusted land which lies marginally above the mean sea level (~4 m). Whereas the eastern GRK primarily receives seasonal fluvial contribution from the Luni river, the western GRK is inundated by storm tides during the southwest Indian monsoon (Glennie and Evans, 1976), and receives water from the ephemeral Nara river during flooding in the Indus (Fig. 4.1), channelized through man-made canals (Syvitski et al., 2013). The desolate landscape of the GRK was not always like this. It is hypothesised that the GRK was a former gulf of the Arabian sea and recurrent seismic activities caused the Rann surface to uplift and finally dry up (Merh, 2005). The archaeological evidence of several Harappan settlements around the GRK points to its eventful past. It is believed that the urban Harappan people had settled down in the semi-arid GRK during 4600-3900 yrs BP (Lindstrom, 2013; Rajesh, 2011) and were using the shallow navigable sea of the Rann, for their maritime activities (Gaur et al., 2013). The remains of one of the largest Harappan acropolises at Dholavira, located in the island of Khadir in the very heart of GRK, bear the testimony of highly active past of the GRK. For the sustenance of human settlements, availability of fresh water as well as connectivity to outer world is very important, however, the present conditions of GRK do not satisfy these conditions.

Moreover, in the previous chapter we have discussed about the fluvial past of the Ghaggar-Hakra river and its connection to the development and decline of the Harappan civilization. The remains of Harappan settlements around the GRK and along the Nara river channel (Fig 4.1), led to the suggestion that the Ghaggar-Hakra and Nara perhaps were a continuous and perennial fluvial system during the mature Harappan period and that the decline of the civilization was triggered by drying up of the river (Misra, 1984; Mughal, 1997; Wright et al., 2008). Indeed some workers, with the help of satellite based studies and historical documents, have identified paleo-river channels that flowed through the present-day arid western margin of the Thar Desert into the Arabian Sea (Ghose et al., 1979; Gupta et al., 2011; Syvitski et al., 2013) and created a delta system in the western Great Rann of Kachchh (Malik et al., 1999). Moreover, a continuous Ghaggar-Hakra-Nara river system has often been equated with the Saraswati, a mythical glacier-fed perennial river (Ghose et al.,

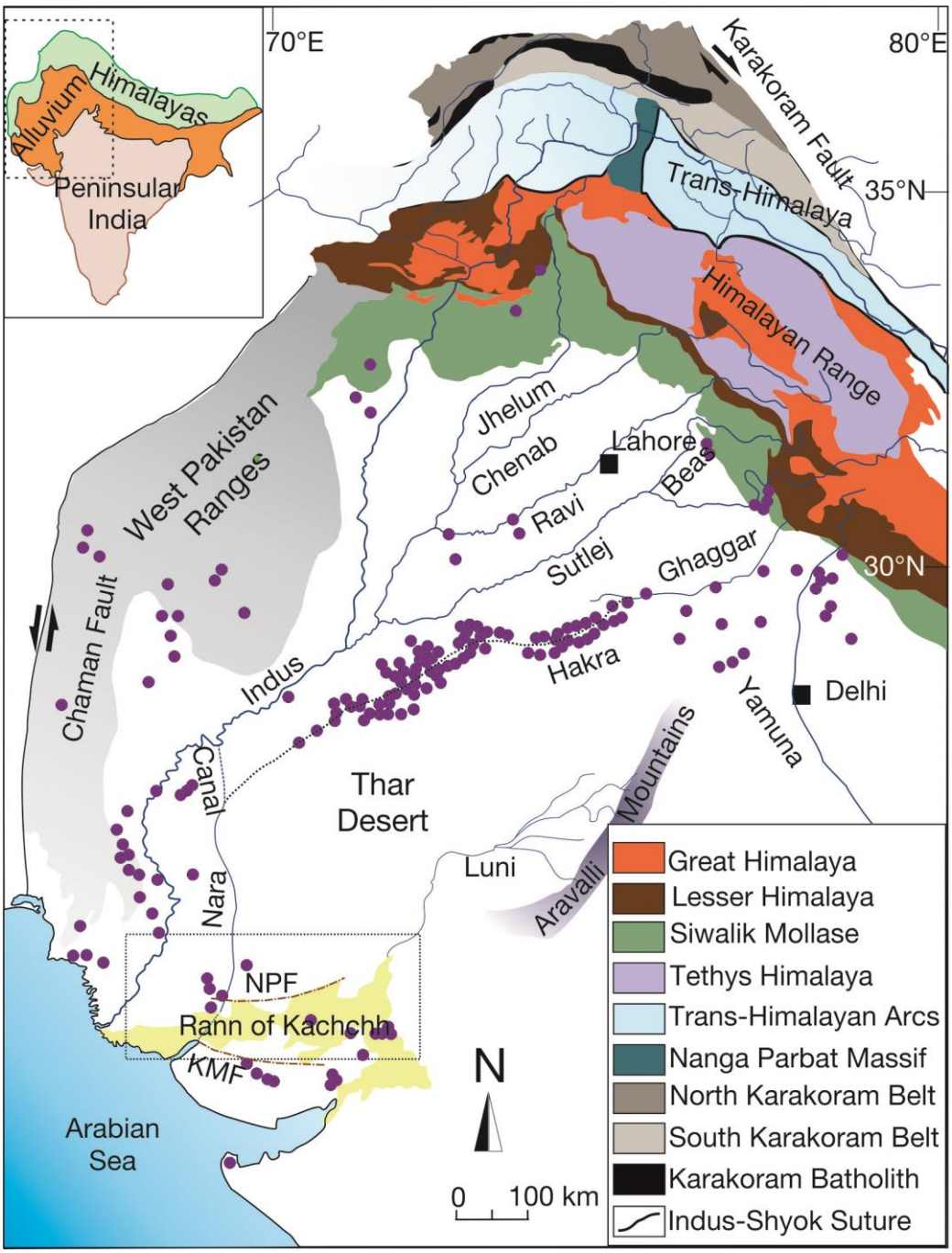

Figure 4.1: Schematic geological sketch map (modified from_Garzanti et al., 2005) showing the major river systems of north-western India and eastern Pakistan (highlighted portion of the map shown in the inset) and lithology of their catchments. Also shown are different geomorphic features/divisions of the region. The dotted line is the speculated major paleochannel (Vedic Saraswati) that connected the Ghaggar with Hakra and Nara during the Harappan period. NPF = Nagar Parker Fault; KMF = Kachchh Mainland Fault. Harappan sites are marked as purple circles.

1979; Kochar, 2000; Oldham, 1893; Pal et al., 1980; Radhakrishan and Merh, 1999; Valdiya, 2013). The sediments exposed in structurally raised sandy mounds ('bet' in local language, Fig. 4.2) and layered sand-silt sediments in the terraces around the margins of the islands (Patcham, Khadir and Bhanjada; Fig. 4.3) bear the testimony of an active fluvial past of the GRK. However, in the absence of robust sedimentological and chronological constrains, the existence of a continuous Ghaggar-Halra-Nara fluvial system flowing into the GRK during the Harappan civilization remains a conjecture. In addition to this, several other workers have suggested that the Nara was only a distributary of the Indus and had no connection to the Ghaggar-Hakra (Alizai et al., 2016, 2011b).

In the above scenario, the Great Rann of Kachchh (GRK) of western India (Fig. 4.2), which is located in the confluence zone between the lost river (vedic Saraswati?) and the Arabian Sea (Valdiya, 2013), becomes an important piece of the puzzle. Therefore, unravelling of the sedimentation history of the GRK since the mid-Holocene, besides being geologically important, has profound geo-archaeological implications towards deciphering the existence of any notable fluvial system (other than Indus) during the proliferation of Harappan civilization. To investigate this aspect of the GRK, we have studied trace element and Sr -Nd isotope geochemistry of sediments deposited in the basin during the last 5.5 kyr, and quantified, for the first time, sediment contributions from various terrigenous sources. We have also made an attempt to decipher sediment transport pathways in order to throw some light on the fluvial scenario of the Harappan period and in the process explored possible existence of a glacial fed river, originating from the higher Himalaya, draining into the Kachchh basin. Our samples came from the relict delta of the river Nara – the purported delta of the Saraswati, central and eastern GRK, mouth of the river Luni, and dunes of the southern-eastern Thar Desert (Fig. 4.2 and 4.3).

4.2 Geology of the Great Rann of Kachchh

The GRK is an enigmatic geomorphic terrain that encompasses a vast stretch of low-lying salty desert (~16,000 sq. km) at the western margin of India, and is devoid of any major drainage; except for the ephemeral river Luni and river Nara – a distributary of the Indus (Fig. 4.1). It is flanked by parabolic dunes in the north and northwest, the Banni Plain and the Wagad Upland in the south (Fig. 4.2). Structurally, the GRK is part of an east-west trending

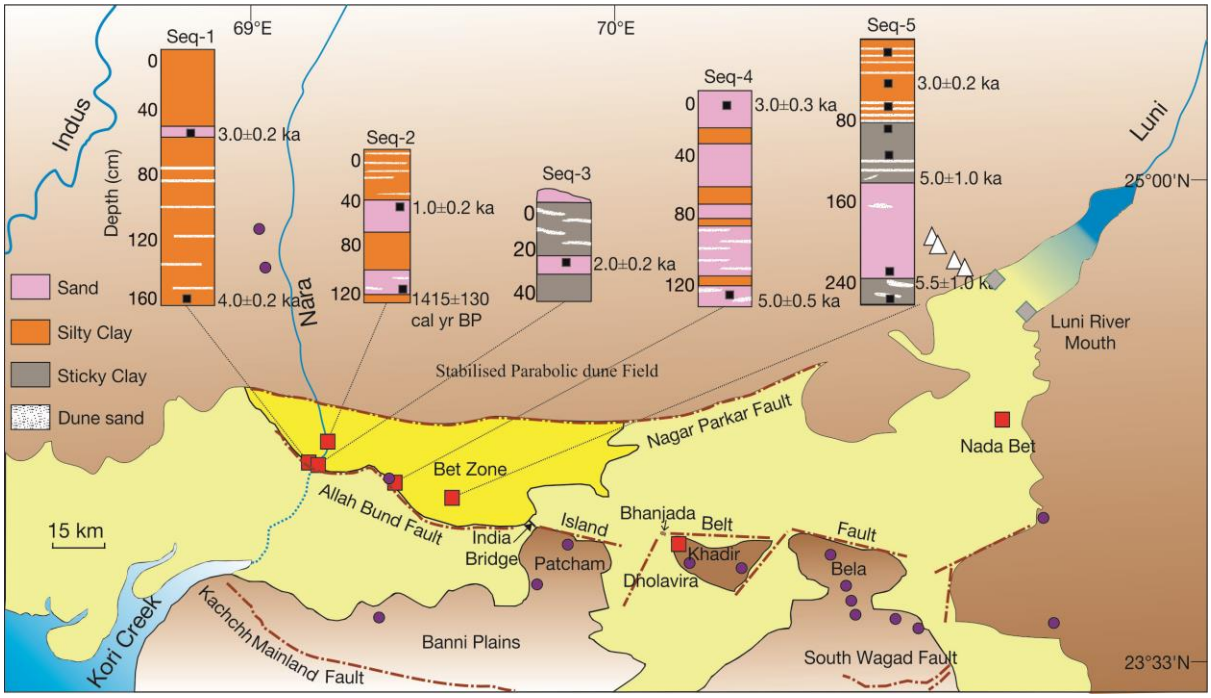

Figure 4. 2: Schematic sketch map (modified from Tyagi et al., 2012) of the blow up of the area marked in (A) showing the major geological/morphological features of the Great Rann of Kachchh (light/dark yellow) and adjoining region. Sampling locations are marked: red squares for Rann (low lands) and bet (uplifted surfaces), grey diamonds for the Luni river mouth, and white triangles for the Thar dune field. Also shown is the stratigraphy of the sedimentary sequences of the sampled horizons (Seq-1 through Seq-5) in the western Great Rann of Kachchh with OSL/radiocarbon ages marked (in ka/cal yr BP). Positions of the samples on the stratigraphic columns are marked as black squares.

paleo-rift graben believed to have formed in the Early Mesozoic (Biswas, 1987) and is bounded in the north by the Nagar Parkar Fault and in the south by the Kachchh Mainland and the South Wagad faults (Fig. 4.2). In between, there exist two other east-west trending faults; namely the Allah Bund and Island Belt (Fig. 4.2), which are known to have influenced the Quaternary morphology of the GRK (Mathew et al., 2006; Maurya et al., 2008; Rajendran and Ranjendran, 2001). It has been suggested that the present day Rann surface is an uplifted floor of a former shallow marine gulf of the Arabian Sea that had formed during sea level rise at the immediate aftermath of the last glacial period (Maurya et al., 2008; Merh, 2005; Oldham, 1926).The latest uplift is believed to have occurred at ~2 kyr ago (Tyagi et al., 2012).

Monotonously flat topography, except for small bets, makes it difficult to determine the history of sedimentation in the western part of the GRK. It is believed that much of the

Holocene sediments in the western part of the basin were derived from the Indus and Nara rivers that once flowed into the basin (Glennie and Evans, 1976). Modern silty-clay deposits are attributed to storm tides, which bring in material from the Indus Delta aided by long-shore current, during the southwest monsoon (Glennie and Evans, 1976; Tyagi et al., 2012). The Banni Plain, which receives sediments from the Mesozoic sedimentary rocks of the northern Kachchh Mainland (Glennie and Evans, 1976; Maurya et al., 2013; Fig. 4.2), acts as a buffer between the Mainland and the western GRK. Considering that the dry highlands and deserts surround the entire GRK, it is reasonable to expect aeolian contribution in the Rann sedimentation during periods of intense wind activity.

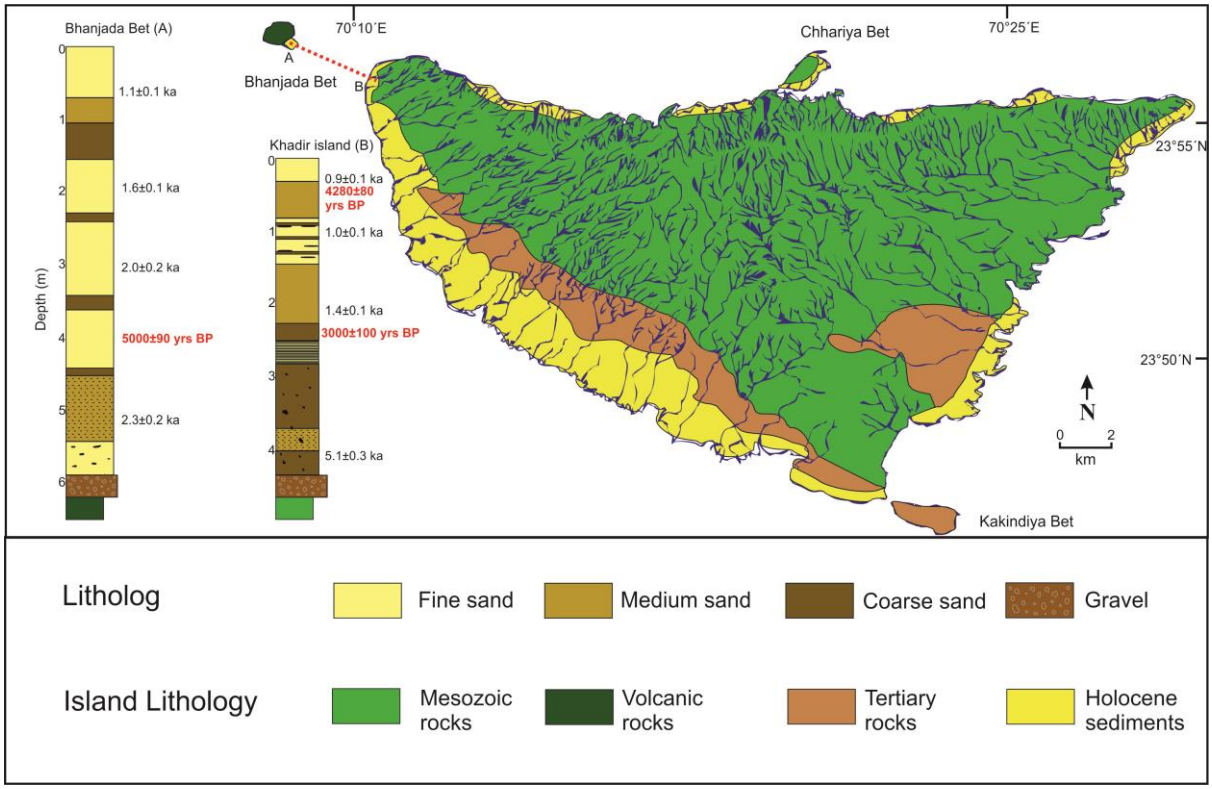

Figure 4. 3: A geological map of Khadir island showing the different lithologies exposed and the drainages present on the island (modified after Ngangom et al., 2017). Also presented is the lithologs of alluvium, exposed around the western margin of the island and eastern margin of the Bhanjada island (modified after Ngangom et al., 2016). The OSL depositional ages reported by Ngangom et al., 2017 are mentioned beside the lithologs. C-14 ages of inorganic (carbonate) carbon from bulk sediment samples measured in the present study are also presented along the lithologs, in red colour.

Unlike western GRK the eastern part has rocky islands made up of Mesozoic and Tertiary rocks (Biswas, 1987). Bela, Khadir and Patcham islands are the major ones. At present, the central and eastern GRK remains detached from the western GRK, along a

median high that passes through north-west of the Patcham Island along the India Bridge (Fig. 4.2). Alluvial successions can be observed along the margins of these rocky islands, especially the Khadir and Bhanjada islands. Both north and south flowing rivers drain the Khadir island from its northern escarpment (Fig. 4.3). The alluvial successions are preserved along the western margin of the Khadir and along the eastern margin of the Bhanjada, which is a sub-volcanic plug (Fig. 4.3). However, the origins of these alluvial successions are debated. Whereas Khonde et al., (2011) suggest that these horizons are tectonically raised Rann sediments, Ngangom et al., (2016) classify them as fluvial deposits.

Tectonically, the GRK is an active landform (Rajendran and Rajendran, 2003; Rajendran and Ranjendran, 2001) . The western GRK had seen one of the largest earthquakes of this region (M_W 7.9) in 1819 that created the Allah Band Fault Scarp. In comparison, the eastern part of the GRK is tectonically less active and there are no historical records of major earthquakes in this region especially during the Harappan times (Rajendran et al., 2008).

4.3 Stratigraphy and Sample Details

4.3.1 Sampling in the Kachchh Basin

- *Western Great Rann of Kachchh*: Sediment samples for the present study were collected from tectonically raised surfaces or terraces, incised channels and dug up trenches (Fig. 4.2). Since the primary focus of the study was the purported delta of the mythical river, we planned to examine in detail the bet zone north of the Allah Bund Fault scarp (Fig. 4.2). Samples from this zone came from five sequences in five locations, in the western GRK, which were topographically higher than the present-day high tide strands. Figure 4.2 presents stratigraphy of these horizons and the already known depositional ages from the work of Tyagi et al., (2012). Three of the sampling locations were on or near the channel of the river Nara (Fig. 4.2).
- *Eastern Great Rann of Kachchh*: Samples representing the central and eastern GRK were collected from the western periphery of Khadir Island and from Nada Bet (Fig. 4.2 and 4.3). These sediments are exposed on fault controlled terraces, which occur as sandy deposits in the centre of silt dominated GRK basin. Figure 4.3 presents the stratigraphy of the alluvium exposed along the Khadir and Bhanjada islands (Fig. 4.4) and their depositional

ages from Ngangom et al., (2016). The alluvium of the eastern GRK varies significantly in grain size compared to that of the western GRK. The eastern GRK sediments are sand dominated, whereas, the western GRK sediments are silt and clay dominated with occasional occurrences of sandy horizons. Sub-recent sediment samples were also collected from the channels inside the Khadir island.

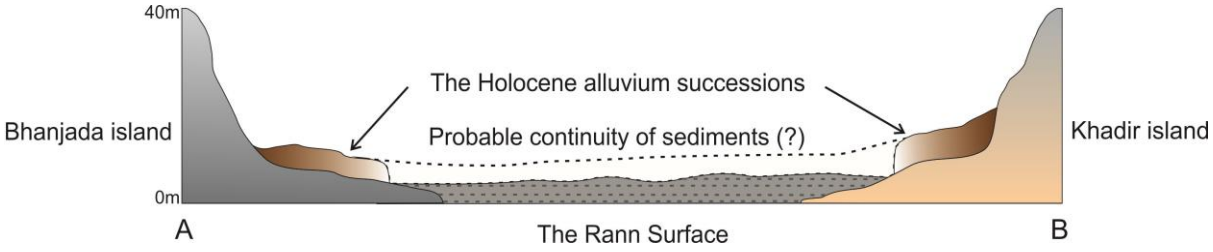

Figure 4.4: A schematic cross-section of the sedimentary successions along the AB line marked in the figure 4.3.

4.3.2 Sampling of Sediment Sources

Apart from the river Nara, other potential sources of sediments to the western GRK during the mid-Holocene include the Thar Desert, the Luni river, the Indus and the Mesozoic rocks of the rocky islands along the GRK.

- *The Thar Desert*: The Thar Desert occurs as the most dominant landscape along the northern margin of the basin. In absence of any major fluvial system from the desert into the Great Rann of Kachchh basin, the only mode of sediment transportation from the north could have been through wind. There was a need to characterize this source as only limited geochemical data existed that too from the far north-eastern margin of the desert, located ~800 km inland (Tripathi et al., 2013). In any case, the dune field at this margin cannot be considered as a potential aeolian sediment source for the GRK since the southwest monsoonal winds are believed to be the primary carrier of the desert sand (Singhvi and Kar, 2004). However, aeolian contribution from the sand dunes present in the vicinity of the GRK is more likely through local sand storms and disturbances as they lack directionality. Therefore, to accurately predict sediment contribution from the Thar, we planned to sample sand dunes that are located very close to the northern margin of the GRK. However, because of inaccessibility of the north-western and northern margin of the basin (located in Pakistan),

we could sample only the dunes located along the north-eastern margin (Fig. 4.2). These samples were sub-recent sediments from stabilized parabolic dune field.

- *The Luni River*: The river Luni is the only river system in India that drains from the Aravalli mountain ranges into the GRK (Fig. 4.1). The river currently is ephemeral and has been so since ~8ka (Kar et al., 2001). Therefore, the sediment supply through it takes place only during heavy rainfall events linked to the southwest Indian monsoon. Because of its very nature, sediments transported by the Luni are mostly reworked alluvial and aeolian deposits. To constrain its contribution to the GRK we sampled sub-surface sediments along the river mouth (Fig. 4.2). These samples would likely to provide average compositions of the Holocene sediments transported by the river.
- *The Nara River*: Although the river Nara today brings in sediments from the river Indus into the GRK, there exists no evidence to suggest if the same were true in the past. However, it has been recognized that recycled Indus sediments have been getting into the basin through creeks via tidal currents as suspended load (mostly clay, Tyagi et al., 2012). In this work we make use of the geochemical data of Clift et al., (2010) and Limmer et al., (2012) for such sediments.

- *The Mesozoic rocks of Kachchh*: The Mesozoic rocks exposed along the margin and islands of the GRK can deliver sediments into the basin via numerous seasonal streams draining through these lithologies. For constraining the sediment contributions from the Mesozoic rocks of Kachchh, we have analysed samples from the Khadir, Bela, Patcham islands and the Kachchh Mainland bordering the GRK basin.

4.4 Results and Discussion

4.4.1 Alluvial deposits of Eastern GRK

To understand the paleo-environmental condition of the eastern Great Rann of Kachchh during the Holocene we have studied the sediments deposited along the outer margins of Khadir and the Bhanjada islands. The nature, source and depositional environment of the alluvial deposits exposed along the rocky islands of the eastern GRK are highly debated. Whereas Khonde et al., (2011) argued for a shallow marine deposition of materials transported from a distant source (Indus shelf sediments), Ngangom et al., (2016) argued for

local sources and a fluvial depositional environment for these sediments. However, in the absence of detailed geochemical data it is difficult to arrive to an unequivocal answer. Besides, there are major differences in the depositional ages of these sequences as reported by these studies. In the course of the present work we aimed to constrain the geochemical composition of the local sources and correlate them with that of the sediments deposited along the island margins. The alluvial deposits are sand dominated with intercalated clay horizons and deposited over the Holocene period (Fig. 4.3). The elevated northern parts of the Khadir island are mainly composed of Mesozoic sandstones and the southern fringes are occupied with Tertiary rocks. It can be also observed that there are both south and north flowing channels draining the island.

A cross-section from the north-western fringe of the Khadir island to the Bhanjada island (AB in fig 4.3) is presented in figure 4.4. Based on the field studies we make the following observations. The alluvial sequences were deposited directly over the Mesozoic rocks in both the islands. The silty-clay deposits of the GRK lie in the space between the two islands. The Rann sediments are neither a part of the island alluvial sequences nor do they overlie.

As discussed earlier, understanding the sedimentation history of the deposits along the Khadir island has archaeological importance too. It is of great importance to understand the depositional environment of alluvium deposited on the perimeter of the Khadir island (marine vs. fluvial) during the Harappan period (mid-Holocene) because, this has a direct implication on the maritime activity of the Harappans.

4.4.1.1 Provenance of alluvial deposits of Khadir and Bhanjada islands

Figure 4.5 presents ε_{Nd} vs $^{87}Sr/^{86}Sr$ plot of the Quaternary alluvial sediments and Mesozoic rocks of the Khadir and Bhanjada islands. The Sr-Nd isotopic composition of the sediments from Khadir region, potteries from Dholavira and Mesozoic rocks are presented in the table 4.1. The plot also shows our data for several other Mesozoic rocks of nearby rocky islands of GRK and in the Kachchh Mainland bordering the GRK. From the figure the following observations and inferences can be made.

- The ~80 ma old volcanic rocks (personal communication from K. Pande) of the Bhanjada island and their weathered horizons have positive ε_{Nd} (0.8 - 2.6) and low radiogenic Sr ($^{87}Sr/^{86}Sr$ = 0.71-0.73).
- The Mesozoic sandstones of Khadir island and other places bordering the eastern GRK have low ε_{Nd} (-15 to -25). These rocks show large spread in their $^{87}Sr/^{86}Sr$ composition (0.71- 0.76).
- The alluvium exposed along the periphery of both Khadir and Bhanjada islands (Fig. 4.4) show overlapping Sr-Nd isotopic compositions indicating their common parentage. The sticky clay deposits of the Rann surface exposed between the two islands have similar isotopic composition as well. The sediments deposited within the island and at the eastern margin of Khadir also possess similar isotopic compositions.
- The observed variation in $^{87}Sr/^{86}Sr$ and ε_{Nd} of these sediments (Fig. 4.5) can be explained by a binary mixing of sediments from the two major island sources present in the vicinity viz. the volcanic rocks of Bhanjada and the Mesozoic sandstones. However, the dominance of the Mesozoic rocks as sediment source is apparent (70 – 80%, Fig. 4.5).

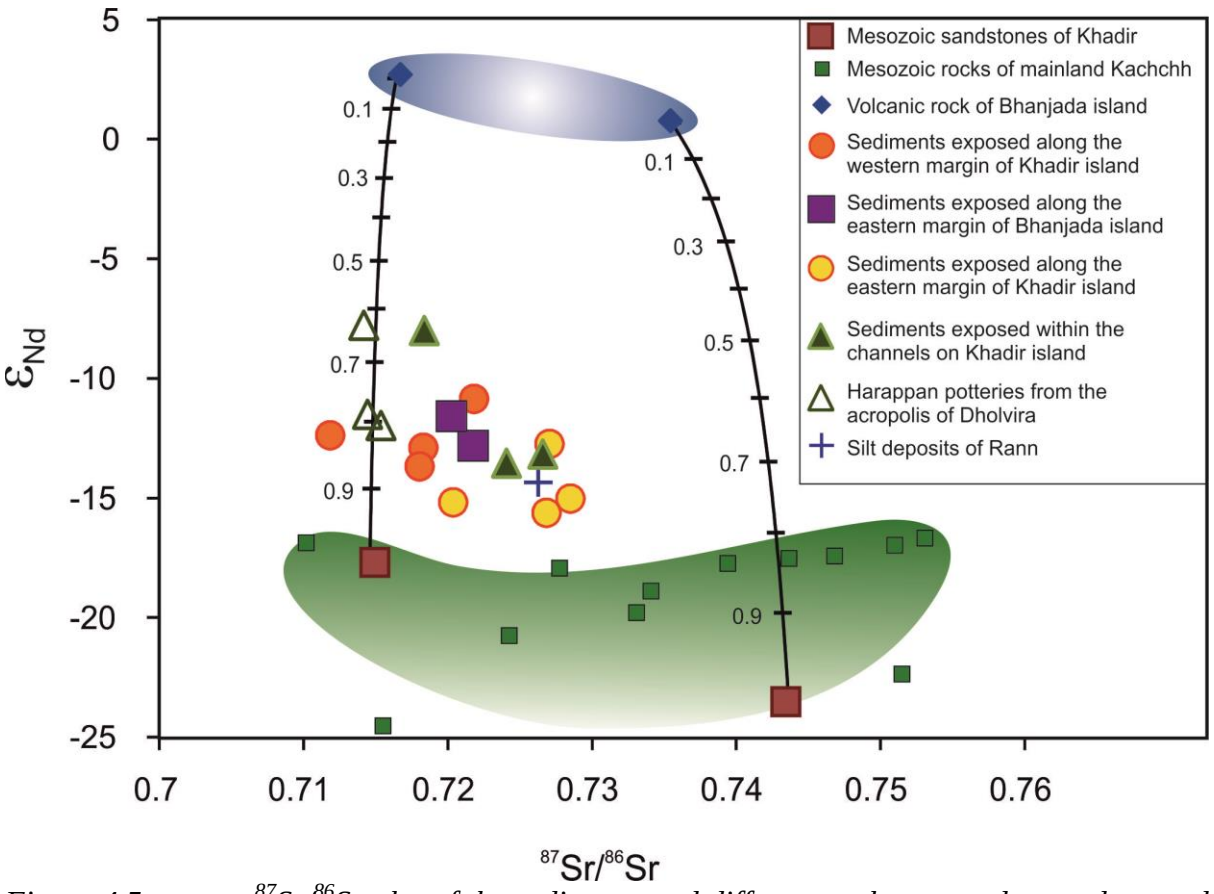

Figure 4.5: ε_{Nd} vs. $^{87}Sr/^{86}Sr$ plot of the sediments and different rocks exposed on and around the Khadir island of the eastern Great Rann of Kachchh.

- Therefore, the sediments deposited around the Khadir island of eastern GRK are clearly locally derived. There is no need to invoke any far-away source to explain the chemical composition of these alluvial deposits.
- Indirect inferences on the sediment provenance for the alluvial deposits can be derived from the isotopic compositions of the Harappan potteries found in the acropolis of Dholavira on Khadir. As discussed in the earlier chapter, the ancient potters generally used local materials to prepare their potteries. Hence, the isotopic composition of the potteries can provide information on the composition of the raw material used and hence the composition of local sediments available during the mid-Holocene period. From the figure 4.5, it can be seen that the potteries have overlapping isotopic composition with the sediments exposed on and around the Khadir island. Even the modern clay horizons found in the seasonal streams around the acropolis of Dholavira have similar compositions. This further confirms that the sediments getting deposited around Khadir island were of local origin, at least since mid-Holocene.

Our inference on the local origin of Khadir sediments is in contradiction with the findings of Khonde et al., (2011), that these alluvial deposits were of marine origin. Their conclusion was based on the presence of abundant foraminifera shells in these sediments. However, the foraminifera shells are abundant only in the topmost part of the sections and the lower parts have very less or no foraminifera shells. In addition Nangom et al., (2016) had argued that these forams do not represent deposition in a marine environment, instead they are reworked from earlier deposits. To resolve this issue, we determined C-14 ages of inorganic (carbonate) carbon from bulk sediment samples from the two horizons exposed along the Khadir and Bhanjada islands. This exercise was done with the assumption that the influx of dead carbon into the system, in form of detrital carbonates from surrounding Mesozoic rocks, had remained constant throughout. Our study revealed that the sediment horizons with very little foraminifera tests have C-14 ages of 3000±100 yrs BP and 5000±90 yrs BP in the Khadir and Bhanjada islands respectively (Fig. 4.3). The zone of maximum abundance of foraminifera at Khadir island yielded an age of 4280±80 yrs BP.

The topmost horizon with abundant foraminifera shells gives an older age than the stratigraphically older sediment layer located 3m below (Fig. 4.3). Therefore, it can be suggested that the forams found in the topmost sediment horizon are mostly reworked fossils

from older deposits. This is not in accordance with the conclusion of Khonde et al., (2011) that the forams grew in situ and the depositional environment around the Khadir island was marine. Earlier Rao et al., (1989) demonstrated how fossil forams originating from the coastal regions of Arabian Sea and the Great Rann of Kachchh as well as from the fossil bearing Tertiary rocks, can be transported in suspension by wind, into the interiors of the Thar desert without getting abraded. Probably, following the same transport mechanism reworked fossil forams were deposited along with the locally derived sediments of the Khadir island. This further indicates that the sediment depositional environment around the Khadir island was probably not marine. Estuarine condition prevailed in that region where sediments transported by local streams got deposited along with the reworked foraminifera shells.

In figure 4.6 a model for the sedimentary environment that prevailed since the mid-Holocene, around the Khadir island is presented. The key inferences on the evolution of the basin are presented below:

- During the mid-Holocene when the sea level was higher in the GRK, the streams flowing through the rocky island of Khadir were depositing their sediments all around the island before meeting the sea further to the west. The depositional environment was most probably estuarine. Overlapping chemical compositions of sediments all around the island as well as those away from the island are the evidence of this wide-spread deposition of locally derived sediments in the eastern GRK.
- Due to the gradual uplift of the Rann surface, the sea started receding since 2000 yrs BP. The local streams then incised the older deposits to reach the sea located further to the west. This caused a lot of older sediments to get eroded away exposing the Rann surface below. The remnant of these deposits remained as the alluvial sequences along the island peripheries (Fig. 4.4).

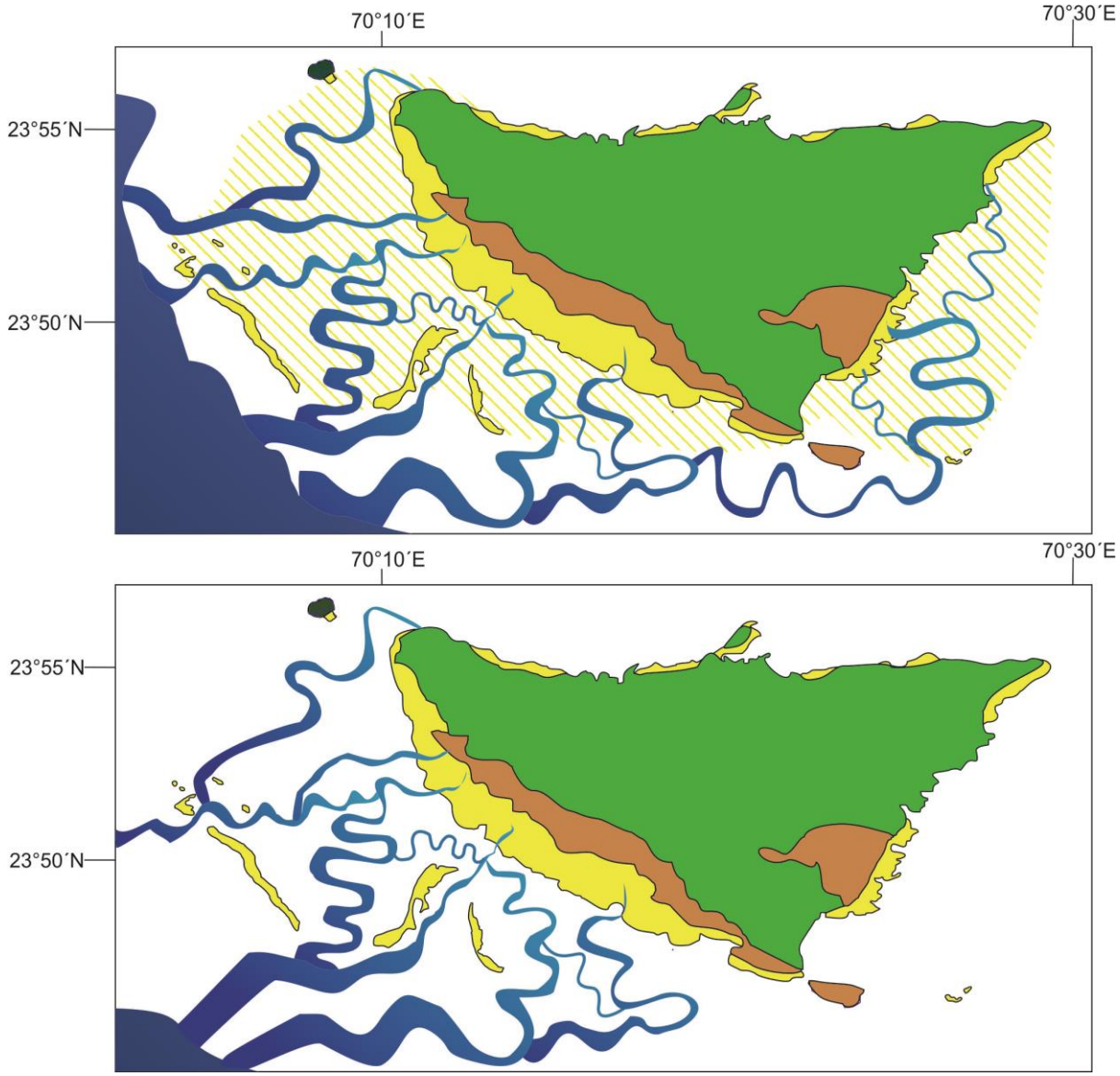

Figure 4.6: (A) A schematic representation of the sedimentation at the eastern GRK during 5-1 Ka. The sea was probably near the western part of the Khadir island and the streams which used to drain the island deposited their sediments in the vicinity of the island, probably in an estuarine condition.
(B) When the sea retreated further west, the streams incised the older sediments to reach the sea and in that process eroded most of the older alluvium, only leaving behind a few remnant cliffs around the Khadir.

4.4.2 Alluvial deposits of the Western Great Rann of Kachchh

4.4.2.1 Geochemistry of siliciclastic sediments

Our geochemical and isotopic data for bulk sediment samples and different grain size fractions from them are presented in Table 4.2 and Table 4.3, respectively. Figure 4.7 presents various trace element and isotopic plots for the sediments deposited in the western GRK. Following observations can be made from these figures.

- The chondrite normalized REE patterns (Fig. 4.7A) for the GRK sediments show pronounced light REE (LREE) enrichment and a negative Eu anomaly - characteristics of continental crust derived detritus.
- The upper continental crust normalized patterns of the sediments (Fig. 4.7B) show a flat LREE and depleted heavy REE (HREE) patterns. The latter possibly hints at removal of heavy minerals such as zircon from sediments prior to their deposition in the basin.
- Negative anomalies of Zr and Hf and depleted patterns of HREE seen in the Post Archean Australian Shale (PAAS) normalized trace element data for these samples (Fig. 4.7C) are consistent with the above observation.
- Interestingly, these patterns are, to a large extent, comparable to that observed in the sediments in the five major rivers of Punjab (Alizai et al., 2011b) and sand dunes of the Thar. These, however, are different from that reported for the sediments from the Indus Delta (Clift et al., 2002, Fig. 4.7C). This is at variance with the earlier belief that the western GRK is predominantly filled with the Indus derived sediments (Maurya et al., 2003; Tyagi et al., 2012). To further understand the nature of probable sediment sources we have made use of various cross plots of elemental and isotopic ratios wherein the fields of these sources (end-members) could be easily distinguished (Fig. 4.7D-F).
- Sediments from the Indus is known to enter the western GRK through the Kori Creek during storm tides with the help of long-shore currents, and having significant contributions from the juvenile (mantle derived) rocks of the Indus-Tsangpo Suture Zone (ITSZ). These have higher Nb/Ba, Cr/Th, ε_{Nd} and Sr content, and lower $^{87}Sr/^{86}Sr$ and Th/Y compared to the Higher-Himalaya-derived sediments in the five rivers of Punjab. Absence of adequate geochemical data does not allow us to create a field/envelope for the Thar Desert; however, we make use of our data from the dune field at the north-eastern margin of the GRK for

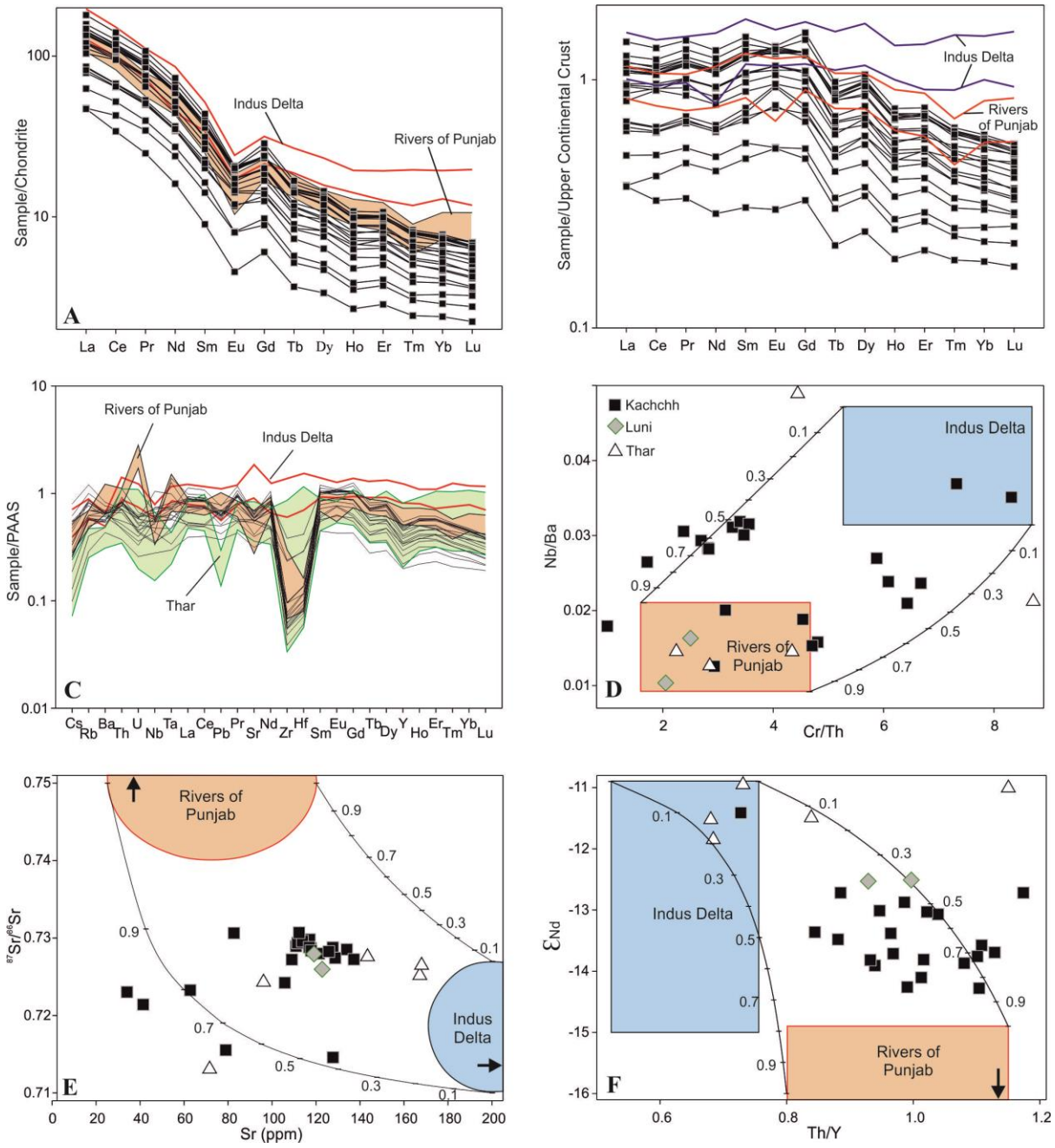

Figuer 4.7: (A) Chondrite normalised, (B) Upper Continental Crust normalised and (C) PAAS normalised multi-element trace element patterns of sediment samples from the Great Rann of Kachchh (this work) compared with that of sediments from rivers of Punjab (Orange field; Alizai et al., 2011a), Indus delta sediments (red envelop; Clift et al., 2002), and Thar desert sand (green field; this work).
(D) Nb/Ta vs. Cr/Th (E) $^{87}Sr/^{86}Sr$ vs. Sr, and (F) ε_{Nd} vs. Th/Y plots for the Kachchh, Luni and Thar samples compared with binary mixing model curves drawn considering sediments in Indus delta and rivers of Punjab as two end-members. Tick marks on mixing curves are fraction of Punjabi rivers' contributions to the mixture.
All the diagrams are modified from Chatterjee and Ray, (2017b).

comparisons. In these plots most of our samples fall in the space in-between the two major end-members (Fig. 4.7D-F) suggesting contributions from all of these sources, not just the Indus, to the sediment budget of the GRK.

Being rare-earth elements, the Sm-Nd isotopic system does not easily get disturbed by the surficial processes like erosion, transportation and sedimentation (Goldstein and Jacobsen, 1988; Najman, 2006). Therefore, this systematics is ideal for provenance study using bulk sediments. The measured ε_{Nd} of samples (with a precision of ±0.2 at 2σ) from the western GRK, the southern Thar Desert and the Luni river mouth varies in ranges of -14.3 to -11.4, -11.8 to -11.0, and -12.5 to -11.5, respectively. In figure 4.8, we compare these data with that from the Holocene sediments in the Ghaggar-Hakra channels, Indus delta and Indus shelf (Alizai et al., 2011a; Clift et al., 2008; East et al., 2015; Limmer et al., 2012; Singh et al., 2016a). From the figure the following inferences can be made.

- It can be inferred that since mid-Holocene there has been little influence of Sutlej or Yamuna in the western GRK sedimentation thus excluding the possibility of the sediments being transported by the Higher Himalayan, glacier-fed rivers.
- On the contrary, ε_{Nd} of the GRK sediments overlap with that observed in the north-eastern Thar Desert, deposited during 9.1 to 1.8 ka (Fig. 4.8A). However, as discussed in the previous section, the only possible mode by which this distal source could have contributed is through reworking by a fluvial system. The present-day ephemeral Ghaggar-Hakra river system, which is believed to have been connected to the Nara during the mid-Holocene (Valdiya, 2013), is the most suitable candidate for the above pathway. The overlapping ε_{Nd} values of pre-modern sediments in the Ghaggar-Hakra system with that of the western GRK sediments (Fig. 4.8B) may be considered as an evidence for the above.
- It is also observed that ε_{Nd} data of the GRK sediments overlap with that of the sediments in the Indus delta (Fig. 4.8B), however, they do not follow the regional trend (with age) shown by the latter thus making it an unlikely source.
- The trend seen in the GRK data (Fig. 4.8B) appears to suggest mixing between sediments from the Ghaggar-Hakra fluvial system (containing reworked aeolian sand from northern desert margin) and Indus borne detritus, in addition to possible contributions from the Luni and the southern Thar (Fig. 4.8A and 4.8B).

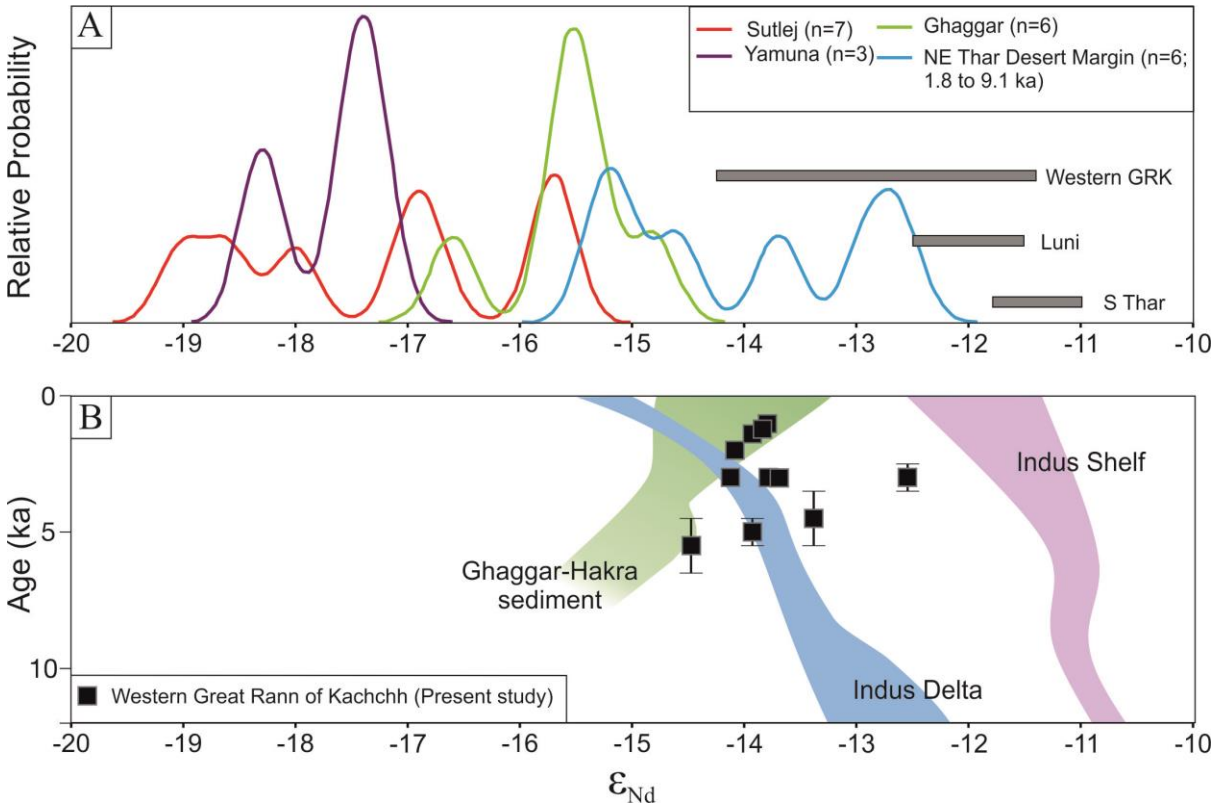

Figure 4. 8: (A) Kernel density estimation (KDE) plot of ε_{Nd} re-drawn from (Singh et al., 2016b) displaying the Nd-isotopic variability in Sutlej, Yamuna, Ghaggar and Thar desert (present work and Singh et al., 2016a; Tripathi et al., 2013).
(B) The Western Great Rann of Kachchh sediments deposited since 5.5 ka are compared with the sediments of Ghaggar-Hakra River (East et al., 2015; Singh et al., 2016a), Indus delta (Clift et al., 2010) and shelf (Limmer et al., 2012) deposited during the Holocene.
All the diagrams are modified from Chatterjee and Ray, (2017b).

4.4.2.2 Grain size dependency of isotopic compositions

For a better characterization of the provenances, we utilize Sr isotopic ratios of these sediments along with their Nd isotopic ratios, keeping in mind the limitations of the former (Najman, 2006). It is generally believed that unlike the ^{147}Sm-^{143}Nd isotopic system, the ^{87}Rb-^{87}Sr system is susceptible to chemical weathering, because of selective fractionation of parent element from the daughter which leads to dissimilar Sr isotopic ratio between the source rocks and the product sediments (Meyer et al., 2011). Higher chemical weathering leads to more radiogenic detritus which is largely controlled by higher $^{87}Sr/^{86}Sr$ bearing fine-grained (clay) fraction, primarily derived from high-Rb bearing micas in the source rocks

(Garçon et al., 2014; Meyer et al., 2011). Below we discuss the effect of grain size on Sr isotopic composition of the GRK sediments and evaluate its bearing on determination of provenances.

Six western GRK samples were selected for studying the effect of grain size on the $^{87}Sr/^{86}Sr$ variation. Different grain size fractions were separated namely: clay (<4μ), silt (4-15.6μ), fine sand (45-75μ) and coarse sand (75-90 μ). By weight coarse sand was found to be the dominant fraction (> 70%) in these samples. All the fractions were decarbonated using dilute HCl before being analyzed for Sr isotopic compositions. These data are plotted in Figure 4.9. As can be seen from the plot, although there is a large variation of $^{87}Sr/^{86}Sr$, our data show an overall increasing $^{87}Sr/^{86}Sr$ value with increasing grain size (Fig. 4.9A). This is entirely opposite of what is generally observed in most fluvial systems wherein the finest fractions (suspended load/clay) contain more radiogenic Sr than the coarser fractions (Garçon et al., 2014).

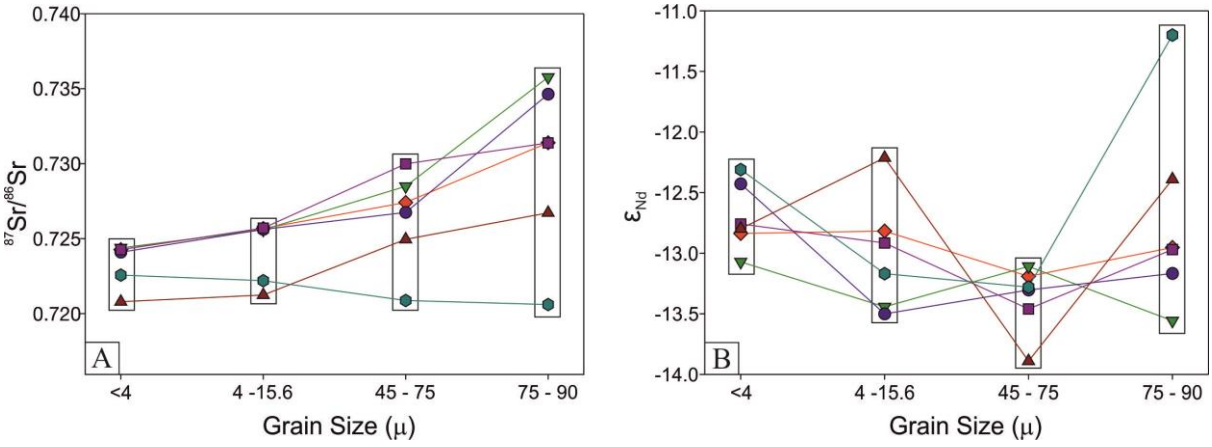

Figure 4.9: (A) Variation of $^{87}Sr/^{86}Sr$ ratio in different grain size fractions (clay, silt, fine and coarse sand) of sediments from Nara river mouth and bet zones are shown. Also plotted are Sr-isotopic ranges of various probable sources. The different symbols represent six separate samples.
(B) Variation of ε_{Nd} values in different grain size fractions of the same sediments mentioned above. The different symbols represent six separate samples.
All the diagrams are modified from Chatterjee and Ray, (2017b).

One plausible explanation for the GRK data could be that different sources with distinct isotopic signatures contributed to different grain size fractions. However, such a phenomenon should have been reflected more prominently is Nd isotopic compositions,

because ε_{Nd} is a more robust provenance indicator compared to $^{87}Sr/^{86}Sr$. However, we do not observe any such dependency in Fig. 4.9B. In fact, a closer look reveals that different grain size fractions of four samples show overlapping ε_{Nd} (within ±0.5, where experimental reproducibility is ±0.2 at 2σ). We therefore believe that the observed variation of $^{87}Sr/^{86}Sr$ ratios with grain-size (Fig. 4.9A) is a product of lesser chemical weathering compared to physical weathering in the source, similar to that observed in many parts of the Himalaya (Singh et al., 2008). Since during chemical weathering, high-Rb bearing minerals (containing high radiogenic Sr) in the source (e.g., muscovite; K-feldspar) break down to clays, finer fractions of sediments produced exhibit higher $^{87}Sr/^{86}Sr$ compared to that in coarser fractions (Garçon et al., 2014). Interestingly, however, we encountered significant amount of muscovite in coarser fractions of our samples, which prompted us to make the above inference. In such a scenario, the $^{87}Sr/^{86}Sr$ of the clay fractions in our samples might not represent the composition of the sources, and therefore, the use of bulk sediment composition for provenance study.

4.4.2.3 Provenance of sediments and implications

- The sediment load of the Indus in its upper reaches, north of its confluence with the rivers of Punjab (Fig. 4.1), is dominated by material derived from sources in the Trans-Himalayas and its Sr-Nd isotopic compositions (IS: Indus at Skardu; Fig. 4.10A) are largely controlled by sediments derived from the ITSZ, Karakoram Batholith, and Ladakh Batholith (Clift et al., 2002).
- Sediments in the Indus delta and shelf (Fig. 4.10A) possess less radiogenic Nd (more radiogenic Sr) compared to that in sediments in the upper Indus. This is due to mixing with sediments from much older crustal rocks in the Higher Himalayan Crystalline (HHC) and Lesser Himalayas (LH), contributed through the rivers of Punjab (Clift et al., 2010).
- The sediments of the GRK having $^{87}Sr/^{86}Sr$ in the range of 0.7146 to 0.7307 and ε_{Nd} in the range of -14.3 to -11.4 although overlap with the field for the Indus Delta (Fig. 4.10A), mostly possess more radiogenic Sr - a characteristic feature of the Lesser and Higher Himalayan sediments.
- The Luni and southern Thar (bordering the GRK basin) sediments have comparable ε_{Nd} and marginally higher $^{87}Sr/^{86}Sr$ values than those of the Indus sediments; however, possess more radiogenic Nd than the GRK sediments (Fig. 4.10A).

- These data clearly suggest that the GRK sediments neither represent any of the pure end-members such as the IS, the Luni, the Thar, the HHC, and the LH nor they are exclusively derived from the river Indus in its lower reaches or the Indus shelf. Since most of our samples are from the western GRK and that there was very limited (if any) sediment transport from the eastern GRK into the western GRK in the past (Glennie and Evans, 1976), the river Luni could not have been a major sediment source or pathway for the latter. Persistent ephemerality and aeolian activity from 8 ka onwards in the Luni basin (Kar et al., 2001), and dissimilar isotopic compositions of the Luni sediments with those of the western GRK sediments (Fig. 4.10A) also support this inference.
- A three component mixing model involving compositions of the IS, HHC and LH (Fig. 4.10A) reveals that although the GRK sediments deposited between 5.5 and 1.0 ka contain a large Trans-Himalayan component (up to 70%), there exists a significant component of the combined Higher and Lesser Himalayan sources. The Trans-Himalayan component can easily be explained by the deposition of the Indus sediments (in lower reaches), directly or reworked, via the Thar desert, and/or through storm tides entering into the western GRK through the Kori Creek that brings in silt and clay from the Indus delta with the help of long-shore currents. It should be noted that although the river Indus transports HHC-LH sediments contributed to it through its eastern tributaries, $^{87}Sr/^{86}Sr$ of the bulk sediments is lowered by a significant non-radiogenic Trans Himalayan component in the main channel - which is reflected in the isotopic composition of the Indus Delta (Clift et al., 2010).
- We, however, observe higher $^{87}Sr/^{86}Sr$ values (> 1.3%) in the sediments of western GRK (Fig. 4.10A), which suggest that there could have been other sources than the river Indus. Since in the present geomorphic set up, direct deposition of the HHC-LH derived sediments into the basin is not possible, contribution from a third source is envisaged.

As mentioned earlier, the Ghaggar-Hakra channel originating from the Siwaliks, made of rocks derived from the HHC-LH (Tripathi et al., 2013), could have been a pathway for the Himalayan contribution to the GRK basin were through the river Nara in the past. Interestingly, the modern sediments of the Ghaggar, which should have had $^{87}Sr/^{86}Sr$ and ε_{Nd} in the range of that of the HHC/LH (Fig. 4.10A), possess lower $^{87}Sr/^{86}Sr$ and higher ε_{Nd} (Tripathi et al., 2013). This has been attributed to contributions from the Paleogene, sub-Himalayan foreland deposits of the Subathu Group (Tripathi et al., 2013). Assuming that the

nature of various sediment sources has not changed since the mid-Holocene, we evaluated their contributions in the samples studied in this work (Fig. 4.10B).

- It is clear from the figure that the pre-modern sediments of the central and eastern GRK, from the Khadir Island (K) and Nada bet (N), although have Sr-Nd isotopic compositions similar to that of the Indus Delta (or Indus in lower reaches), are most likely derived from the river Luni, the Thar Desert and Mesozoic rocks exposed on the islands. In any case, the local sources do not produce significant amount of sediment and their compositions are very different from that of the western GRK sediments.
- Comparison of our isotopic data with model grids of a three component mixing, where sediments from the Ghaggar, southern Thar and the Indus delta/shelf are the end-members (Fig. 4.10B), suggests that 20 to 30% of the sediments deposited in the western GRK during 5.5 to 1.0 ka could have been delivered through the now-defunct pathway connecting the Ghaggar, Hakra and Nara channels.
- The samples that possess high radiogenic Sr (> 0.728) are both sand and clay rich sediments and these are not confined to any age bracket in the studied period. A large number of them come from fluvially deposited horizons.

If the finding of (Giosan et al., 2012) that there was fluvial activity in the Nara valley ~2.9 kyr ago were to be believed then our younger samples most likely represent monsoonal flooding events. Although the geochemical data for the GRK sediments clearly point towards a significant presence of sub-Himalayan (Siwalik) sediments that are not part of the Indus detritus.The overwhelming presence of the latter and southern Thar sand (up to 70%) makes it apparent that no perennial fluvial system was active in the Ghaggar-Hakra-Nara system during the Mature Harappan period. Our data nonetheless suggest that the Ghaggar-Hakra-Nara channels had remained active, possibly as a monsoon-fed system, until ~1.0 kyr ago. It was a sub-parallel system to the Indus, which transported sediments from the southern flanks of the Himalayas along with reworked aeolian sands into the GRK. Such an inference is not inconsistent with the inferences of (Giosan et al., 2012) and that these channels were active through intermittent flooding during the mid-Holocene, even after a substantial weakening of the monsoon post 4.2 ka (Enzel et al., 1999; Staubwasser et al., 2003; Wünnemann et al., 2010), before being covered by aeolian deposits. Although it is difficult to directly infer about the prevailing climatic conditions from our geochemical study, the sedimentological

observations that substantial fluvial sand was deposited during 5.0-3.0 ka and 1.4-1.0 ka (Fig. 4.2) suggest enhanced rainfall, possibly caused by stronger Indian monsoon. Such an inference is supported by studies that propose short phases of monsoonal strengthening in peninsular India during 5100-4700 ka, 4105-2640 ka, and medieval warm period (Band et al., 2016; Banerji et al., 2016; Ngangom et al., 2012; Sarkar et al., 2000; Yadava and Ramesh, 2005) in the background of a regional decreasing trend since ~7 ka (Dixit et al., 2014; Sarkar et al., 2016).

4.5. Conclusions

Field studies, geochemistry and Sr-Nd isotopic data for mid-Holocene terrigenous detritus from the GRK reveal that the river Luni, Mesozoic rocks on the islands, and parabolic dune field of the south-eastern Thar are the primary contributors of sediments to the central and eastern GRK. The sediments deposited around the rocky islands of eastern GRK are primarily derived from local sources and deposited by seasonal local streams.

On the other hand, sediments deposited in the western GRK during 5.5 to 1.0 kyr ago, although are primarily derived from the river Indus and transported into the basin by storm tides from the Indus delta and/or shelf; contain a significant amount of an independent sub-Himalayan component (30 - 40%). This sub-Himalayan component most likely was transported through the now defunct Ghaggar-Hakra-Nara river system. Since this river system, which ran parallel to the Indus, had dwindling water supply during the Harappan period, sediments carried by it must have reached the GRK only during heavy flooding events. Overwhelming presence of Indus detritus in the GRK makes it difficult to test the hypothesis of existence of a mega, glacial-fed river through the Ghaggar-Hakra-Nara channels during this period. These channels, however, were active until as late as 1.0 ka and therefore, their drying up may not have any causal relationship with the decline of the Harappan civilization.

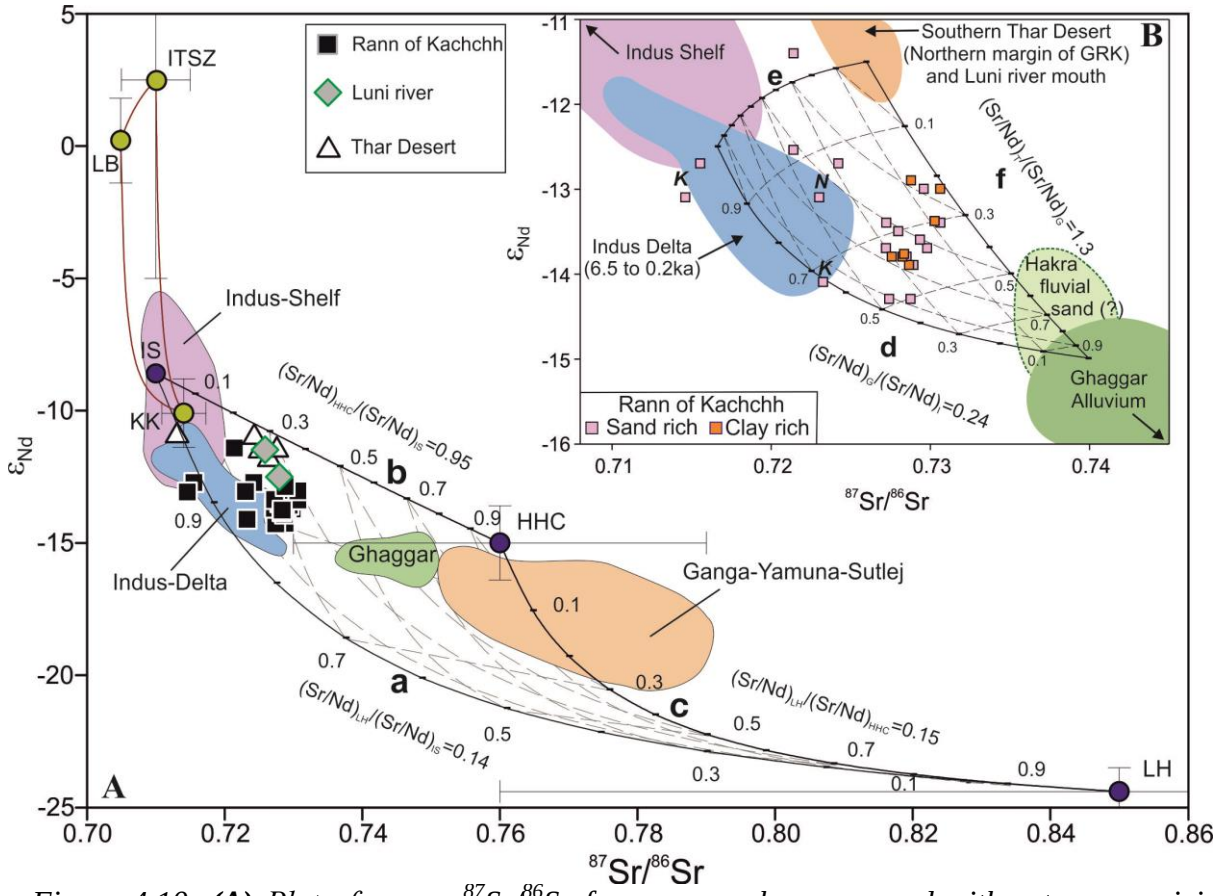

Figure 4.10: ***(A)*** *Plot of* ε_{Nd} *vs.* $^{87}Sr/^{86}Sr$ *for our samples compared with a ternary mixing grid. The three end-members are: (1) Indus sediments at Skardu (IS), (2) sediments derived from the Higher Himalayan Crystallines (HHC), and (3) sediments derived from the Lesser Himalayas (LH). IS component itself plots within another three component mixing grid involving the Indo-Tsangpo Suture Zone (ITSZ), Karakoram (KK) and Ladakh Batholith (LB) as end-members. Error bars cover the entire range of values for various components. Also shown are fields for sediments in the Indus Delta, present-day Ghaggar, and Ganga-Yamuna-Sutlej river systems. Curves a, b, and c represent binary mixing between typical compositions of two each of the end-members, whose compositions are: IS: Nd = 25 ppm; Sr = 210 ppm;* ε_{Nd}*= -8.6;* $^{87}Sr/^{86}Sr$*= 0.71, HHC: Nd = 30 ppm; Sr = 240 ppm;* ε_{Nd}*= -15.0;* $^{87}Sr/^{86}Sr$*= 0.76, and LH: Nd = 100 ppm; Sr = 120 ppm;* ε_{Nd}*= -24.4;* $^{87}Sr/^{86}Sr$*= 0.85. Error bars of end-member compositions are at* 3σ*. The diagram is modified from Chatterjee and Ray, (2017b).* ***(B)*** *Plot of* ε_{Nd} *vs.* $^{87}Sr/^{86}Sr$ *for only the Great Rann of Kachchh samples, compared with a ternary mixing grid involving Indus river sediments, Thar Desert, and Ghaggar. Only* ε_{Nd} *values are available for fluvial sands of Hakra stream*(East et al., 2015). *However considering the fact that, Hakra is the downstream extension of Ghaggar, we have considered the range of* $^{87}Sr/^{86}Sr$ *values for Hakra sediments to be similar to Ghaggar. Hence, the zone defined for Hakra sediments in the figure are question marked. K and N represent samples from the Khadir Island and Nada Bet, respectively, in the eastern Rann of Kachchh (Fig. 1B). Curves d, e, and f represent binary mixing between typical compositions of two each of the end-members and these are: Indus Shelf/Delta: Nd = 30 ppm; Sr = 350 ppm;* ε_{Nd}*= -12.5;* $^{87}Sr/^{86}Sr$*= 0.7166, southern Thar Desert: Nd = 40 ppm; Sr = 150 ppm;* ε_{Nd}*= -11.5;* $^{87}Sr/^{86}Sr$*= 0.726, and Ghaggar: Nd = 100 ppm; Sr = 280 ppm;* ε_{Nd}*= -15;* $^{87}Sr/^{86}Sr$*= 0.740. Data sources: present work and refs (Allègre and Othman, 1980; Clift et al., 2002; Najman, 2006; Scharer et al., 1990; Singh et al., 2016a; Tripathi et al., 2013). The diagram is modified from Chatterjee and Ray, (2017b).*

Table 4.1 Sr-Nd isotopic compositions of sediments from the Khadir island, Bhanjada island, potteries from Dholavira and various Mesozoic rocks.

Samples	Description	$^{87}Sr/^{86}Sr$	e_{Nd}
KH-15-6	White Weathered sandstone (Khadir)	**0.714940**	**-17.7**
KH-15-11	Alkaline Rock (Bhanjada island)	**0.716780**	**2.6**
KH-15-14	weathered Alkaline Rock (Bhanjada island)	**0.735500**	**0.8**
KH-15-27	Yellow sandstone (Khadir)	**0.743415**	**-23.5**
KH-15-27R		**0.743439**	
KH-15-22	Sand near western gully	**0.721850**	**-10.9**
KH-15-28	Silty-sand on Khadir island	**0.726640**	**-13.2**
KH-15-33	sediments from the eastern margin of Khadir	**0.727085**	**-12.9**
KH-15-34		**0.728468**	**-15.1**
KH-15-35		**0.720501**	**-15.3**
KH-15-37	Top fine sand	**0.724140**	**-13.6**
KH-15-23	Rann sediment from the western margin of Khadir	**0.726327**	**-14.4**
KH-15-23R		**0.726325**	
KH-15-40	Rann sediment from the eastern margin of Khadir	**0.726999**	**-15.7**
KH-15-15	Sediments along the western margin of Khadir	**0.718329**	**-12.9**
KH-15-17		**0.718072**	**-13.7**
KH-15-20		**0.711865**	**-12.4**
BJ-15-3	Sediments along the eastern margin of Bhanjada	**0.720350**	**-11.6**
BJ-15-5		**0.721822**	**-12.9**
KH-15-30	Clay from sream around Dholavira	**0.718440**	**-8.0**
DV-1	Dholavira Pottery Samples	**0.713944**	**-11.8**
DV-2		**0.713626**	**-7.9**
DV-3		**0.714845**	**-12.2**
KS-1	Mesozoic rocks of Kachchh mainland bordering the GRK and Paccham island	**0.715403**	**-24.6**
M-61		**0.710273**	**-16.9**
G-1		**0.753146**	**-16.7**
G-2		**0.714821**	**-12.3**
WD-2		**0.733121**	**-19.8**
FS-7		**0.743703**	**-17.6**
DB-1		**0.751619**	**-22.4**
FS-0		**0.739414**	**-17.7**
BHU-1		**0.734185**	**-18.9**
GS-09		**0.724305**	**-20.7**
JUM-1		**0.746849**	**-17.4**
JHN-7		**0.727765**	**-17.9**
JHN-12		**0.751035**	**-17**

Table 4.2: Geochemical data for sediment samples from the Great Rann of Kachchh

Sample	SBTL-1[K]	NRMOSL-1[K]	ABP-1a[K]	KHTL-1[D]	KSTL-1[K]
Cs	1.92	3.84	3.99	8.33	3.97
Rb	64.2	94.4	91.8	123.1	90.4
Ba	313	363	354	402	348
Th	13.5	12.3	16.1	8.1	10.4
U	1.83	1.64	2.07	1.50	1.42
Nb	8	11	11	14	10
Ta	1.77	0.85	0.91	0.93	1.62
La	37	35	43	19	28
Ce	77	72	86	39	58
Pb	12.2	13.1	15.3	8.4	12.8
Pr	9.4	8.5	10.2	4.7	7.1
Sr	128	134	129	79	117
Nd	31	27	33	16	23
Zr	12	13	15	49	11
Hf	0.4	0.4	0.5	1.5	0.4
Sm	6.3	5.7	6.7	3.2	4.8
Eu	1.2	1.1	1.2	0.7	1.0
Gd	5.5	4.9	5.9	2.8	4.1
Tb	0.60	0.53	0.63	0.32	0.46
Dy	3.5	3.1	3.7	2.1	2.7
Y	13.6	12.1	14.6	9.1	10.7
Ho	0.58	0.50	0.61	0.38	0.46
Er	1.6	1.5	1.8	1.2	1.3
Tm	0.2	0.2	0.2	0.2	0.2
Yb	1.2	1.1	1.3	1.0	1.0
Lu	0.16	0.15	0.18	0.15	0.13
Sc	6.7	7.3	8.4	11.0	6.7
V	39	49	56	86	43
Cr	23	33	38	67	29
Co	3	4	5	7	4
$^{87}Sr/^{86}Sr$	0.72878	0.72853	0.72743	0.71553	0.72982
$^{143}Nd/^{144}Nd$	0.511907	0.511930	0.511906	0.511982	0.511935
$\varepsilon_{Nd}(0)$	-14.3	-13.8	-14.3	-12.7	-13.7

Sample	KHTL-3[D]	BBMF[K]	KH/DV/TL1[D]	ABP-2[K]	KSTL-2[K]
Cs	1.48	9.28	3.88	7.57	7.75
Rb	46.2	160.1	73.6	131.9	137.3
Ba	281	497	17	427	426
Th	5.4	10.4	4.8	10.3	9.7
U	0.80	1.36	0.79	1.37	1.33
Nb	5	12	6	7	7
Ta	0.38	0.75	0.38	0.56	0.61
La	15	29	11	29	26
Ce	32	62	26	60	59
Pb	7.4	12.7	3.0	12.2	12.7
Pr	3.8	7.2	3.3	7.2	6.6
Sr	63	109	128	111	112
Nd	12	23	11	23	21
Zr	20	14	18	12	8
Hf	0.6	0.5	0.6	0.4	0.3
Sm	2.5	4.7	2.2	4.8	4.4
Eu	0.5	1.0	0.5	1.0	0.9
Gd	2.0	4.0	1.8	4.1	3.7
Tb	0.21	0.43	0.19	0.43	0.40

Dy	1.3	2.5	1.2	2.5	2.3
Y	5.4	9.2	4.6	9.5	8.7
Ho	0.22	0.40	0.20	0.42	0.38
Er	0.7	1.2	0.6	1.2	1.1
Tm	0.1	0.1	0.1	0.1	0.1
Yb	0.6	0.9	0.5	0.9	0.8
Lu	0.08	0.12	0.07	0.12	0.11
Sc	3.3	12.2	5.6	9.9	9.6
V	33	97	45	77	68
Cr	25	63	32	49	45
Co	2	8	4	7	8
$^{87}Sr/^{86}Sr$	0.72327	0.72723	0.71459	0.72896	0.72937
$^{143}Nd/^{144}Nd$	0.511915	0.511936	0.511968	0.511927	0.511942
$\varepsilon_{Nd}(0)$	-14.1	-13.7	-13.1	-13.9	-13.6

Sample	KRNOSL-3[K]	ABTL-2[K]	SBTL-4[K]	KH/DV/TL2[D]	BdB(b)-1[K]
Cs	0.77	3.79	4.34	5.82	6.60
Rb	39.3	90.4	99.9	99.6	130.6
Ba	201	375	438	394	420
Th	1.3	11.4	11.8	7.0	7.5
U	0.30	1.89	1.84	1.11	1.23
Nb	3	12	14	8	11
Ta	0.13	1.00	1.05	0.43	0.80
La	3	33	34	20	20
Ce	6	68	70	41	41
Pb	8.4	15.6	11.5	10.0	13.8
Pr	0.7	8.3	8.5	4.9	5.1
Sr	41	121	118	106	114
Nd	2	26	27	15	16
Zr	8	16	20	20	13
Hf	0.3	0.6	0.7	0.7	0.5
Sm	0.5	5.7	5.7	3.1	3.5
Eu	0.2	1.2	1.1	0.7	0.8
Gd	0.5	4.9	4.9	2.6	3.0
Tb	0.06	0.56	0.54	0.27	0.34
Dy	0.4	3.4	3.3	1.6	2.1
Y	1.7	13.0	12.6	5.9	7.9
Ho	0.08	0.58	0.55	0.27	0.36
Er	0.2	1.7	1.6	0.8	1.1
Tm	0.0	0.2	0.2	0.1	0.1
Yb	0.2	1.3	1.2	0.7	0.8
Lu	0.03	0.18	0.16	0.09	0.11
Sc	1.2	8.5	8.9	8.1	8.8
V	14	53	60	64	65
Cr	4	37	40	45	44
Co	1	4	3	5	7
$^{87}Sr/^{86}Sr$	0.72141	0.72800	0.72869	0.72423	0.72961
$^{143}Nd/^{144}Nd$	0.512053	0.511947	0.511925	0.511986	0.511971
$\varepsilon_{Nd}(0)$	-11.4	-13.5	-13.9	-12.7	-13.0

Sample	NRMOSL-3[K]	GdB-2[K]	C-16/13[K]	C-16/17[K]	C-16/21[K]
Cs	2.81	7.09	4.97	11.98	5.27
Rb	79.3	136.7	111.2	192.3	111.4
Ba	365	445	429	538	419
Th	11.2	6.8	12.1	10.4	12.0
U	1.79	1.02	1.95	1.79	1.87
Nb	10	11	14	20	13

Ta	0.73	0.73	0.96	1.27	0.92
La	33	19	33	25	32
Ce	67	40	70	58	67
Pb	13.7	13.6	12.7	10.2	12.5
Pr	8.2	4.8	8.3	6.1	8.1
Sr	137	112	126	83	117
Nd	26	15	27	20	25
Zr	12	10	20	50	16
Hf	0.4	0.4	0.7	1.4	0.6
Sm	5.7	3.3	5.7	4.0	5.5
Eu	1.2	0.8	1.2	0.8	1.1
Gd	4.9	2.9	4.9	3.5	4.8
Tb	0.56	0.31	0.55	0.39	0.54
Dy	3.5	1.9	3.4	2.4	3.3
Y	13.3	7.0	13.0	10.2	12.2
Ho	0.58	0.32	0.56	0.45	0.56
Er	1.7	0.9	1.7	1.4	1.6
Tm	0.2	0.1	0.2	0.2	0.2
Yb	1.3	0.7	1.3	1.2	1.2
Lu	0.17	0.09	0.17	0.16	0.16
Sc	7.9	8.6	9.5	13.6	9.8
V	49	61	65	119	69
Cr	32	45	43	76	42
Co	3	6	4	7	4
$^{87}Sr/^{86}Sr$	0.72725	0.73066	0.72832	0.73064	0.72881
$^{143}Nd/^{144}Nd$	0.511953	0.511952	0.511930	0.511970	0.511978
$\varepsilon_{Nd}(0)$	-13.4	-13.4	-13.8	-13.0	-12.9

Sample	C-16/26[K]	NB-1[N]	MS-1[L]	BKS-4[L]	BKS-1[T]
Cs	4.97	0.47	1.46	1.25	1.53
Rb	110.7	23.9	64.6	57.8	55.9
Ba	451	128	340	315	281
Th	12.2	6.0	5.5	8.1	6.7
U	1.58	1.43	0.79	1.12	0.94
Nb	9	2	4	5	6
Ta	0.61	0.06	0.32	0.91	0.55
La	35	11	15	24	23
Ce	73	21	29	50	45
Pb	11.8	4.0	13.0	12.3	4.7
Pr	8.8	2.4	3.5	6.0	4.9
Sr	118	34	119	123	167
Nd	28	7	11	19	18
Zr	80	14	7	10	13
Hf	2.1	0.5	0.3	0.4	0.4
Sm	5.9	1.4	2.2	3.9	3.1
Eu	1.2	0.3	0.6	0.8	0.7
Gd	4.9	1.2	1.9	3.3	2.9
Tb	0.53	0.14	0.22	0.36	0.34
Dy	3.0	0.9	1.4	2.2	2.0
Y	11.1	3.6	5.6	8.7	9.8
Ho	0.50	0.15	0.23	0.37	0.36
Er	1.4	0.5	0.7	1.1	1.1
Tm	0.2	0.1	0.1	0.1	0.1
Yb	1.0	0.4	0.5	0.9	1.0
Lu	0.14	0.06	0.07	0.12	0.13
Sc	9.6	1.6			5.8
V	65	10			41

Cr	38	6	11	20	58
Co	4	1	2	2	3
$^{87}Sr/^{86}Sr$	0.72837	0.72303	0.72794	0.72610	0.72516
$^{143}Nd/^{144}Nd$	0.511933	0.511969	0.511997	0.512050	0.512047
$\varepsilon_{Nd}(0)$	-13.8	-13.1	-12.5	-11.5	-11.5
Sample	BKS-1-CLAY^{T}	BKS-2^{T}	BKS-3^{T}	BKS-5^{T}	BHVO-2
Cs	3.60	1.73	1.65	1.08	0.12
Rb	75.0	64.0	57.0	40.3	10.3
Ba	260	313	280	201	130
Th	16.1	6.3	5.0	6.4	1.1
U	3.37	0.72	0.62	0.63	0.42
Nb	13	5	4	3	17
Ta	0.46	0.47	0.30	0.28	0.95
La	32	21	18	21	15
Ce	78	40	36	41	39
Pb	2.7	5.2	5.9	4.1	1.2
Pr	7.3	4.3	4.0	4.4	5.2
Sr	72	168	143	96	388
Nd	23	15	11	11	24
Zr	181	16	7	13	163
Hf	5.8	0.5	0.3	0.5	3.9
Sm	5.0	2.7	2.6	2.5	5.9
Eu	0.9	0.7	0.8	0.6	2.0
Gd	5.1	2.5	2.4	2.4	6.1
Tb	0.67	0.30	0.28	0.27	0.84
Dy	4.6	1.9	1.6	1.5	5.2
Y	22.0	9.2	6.0	5.5	23.4
Ho	0.92	0.34	0.30	0.29	0.89
Er	3.0	1.1	0.9	0.9	2.5
Tm	0.4	0.1	0.1	0.1	0.3
Yb	3.0	1.0	0.8	0.9	1.9
Lu	0.44	0.14	0.11	0.13	0.26
Sc	9.5	6.1	3.9	3.1	31.6
V	78	32	27	22	337
Cr	71	27	14	14	291
Co	3	3	2	2	48
$^{87}Sr/^{86}Sr$	0.71307	0.72648	0.72758	0.72429	0.70346
$^{143}Nd/^{144}Nd$	0.512077	0.512031	0.512049	0.512074	0.512967
$\varepsilon_{Nd}(0)$	-11.0	-11.8	-11.5	-11.0	6.4

Superscripts: ^{K} = Western Great Rann of Kachchh; ^{D} = Khadir Island, Eastern Great Rann of Kachchh; ^{N} = Nada Bet, Eastern Great Rann of Kachchh; ^{L} = Luni River mouth; ^{T} = Thar dune sand. Trace element concentrations are in ppm.Data for BHVO-2 is averages of 10 analyses. . $\varepsilon_{Nd} = [(^{143}Nd/^{144}Nd)_{sample}/(^{143}Nd/^{144}Nd)_{Chondrite}-1]*10^{4}$. Reproducibility (2$\sigma$): $^{87}Sr/^{86}Sr = \pm 0.000005$; $\varepsilon_{Nd} = \pm 0.1$For $\varepsilon_{Nd}(0)$ calculation a value of 0.512638 was taken for present-day $^{143}Nd/^{144}Nd$ for chrondrite meteorite.

Table 4.3: Isotopic data for different grain sizes separated from sediments of the Nara river mouth and Western Great Rann of Kachchh

<4μm	NRM-OSL-1C	NRM-OSL-2C	NRM-OSL-3C	KRM-OSL-1C	KRM-OSL-2C	KRM-OSL-3C
$^{87}Sr/^{86}Sr$	0.72427	0.72438	0.72409	0.72427	0.72079	0.72257
$^{143}Nd/^{144}Nd$	0.51198	0.511968	0.512001	0.511984	0.511982	0.512007
$\varepsilon_{Nd}(0)$	-12.8	-13.1	-12.4	-12.8	-12.8	-12.3

4-15.6 μm	NRM-OSL-1S	NRM-OSL-2S	NRM-OSL-3S	KRM-OSL-1S	KRM-OSL-2S	KRM-OSL-3S
$^{87}Sr/^{86}Sr$	0.72568	0.72559	0.72562	0.72570	0.72124	0.7222
$^{143}Nd/^{144}Nd$	0.511981	0.511949	0.511946	0.511976	0.512012	0.511963
$\varepsilon_{Nd}(0)$	-12.8	-13.4	-13.5	-12.9	-12.2	-13.2

45-75 μm	NRM-OSL-1A	NRM-OSL-2A	NRM-OSL-3A	KRM-OSL-1A	KRM-OSL-2A	KRM-OSL-3A
$^{87}Sr/^{86}Sr$	0.72741	0.72849	0.72674	0.72999	0.72495	0.72087
$^{143}Nd/^{144}Nd$	0.511962	0.511966	0.511956	0.511948	0.511926	0.511957
$\varepsilon_{Nd}(0)$	-13.2	-13.1	-13.3	-13.5	-13.9	-13.3

75-90 μm	NRM-OSL-1B	NRM-OSL-2B	NRM-OSL-3B	KRM-OSL-1B	KRM-OSL-2B	KRM-OSL-3B
$^{87}Sr/^{86}Sr$	0.73140	0.73576	0.73463	0.73138	0.72672	0.72060
$^{143}Nd/^{144}Nd$	0.511974	0.511943	0.511963	0.511973	0.512003	0.512064
$\varepsilon_{Nd}(0)$	-12.3	-13.6	-13.2	-13.0	-12.4	-11.2